Self-pulsing dynamics in a cavity soliton laser

T. Ackemann, N. Radwell, C. McIntyre, W. J. Firth, and G.-L. Oppo

SUPA and Department of Physics, University of Strathclyde, Glasgow G4 ONG, Scotland, UK

T. Ackemann, N. Radwell, C. McIntyre, W. J. Firth, and G.-L. Oppo. "Self-pulsing dynamics in a cavity soliton laser." Semiconductor Lasers and Laser Dynamics IV, K. Panajotov, M. Sciamanna, A. A. Valle, R. Michalzik (editors). Proc. SPIE **7720**, 772007, 2010.

http://dx.doi.org/10.1117/12.854039

ABSTRACT

The dynamics of a broad-area vertical-cavity surface-emitting laser (VCSEL) with frequency-selective feedback supporting bistable spatial solitons is analyzed experimentally and theoretically. The transient dynamics of a switch-on of a soliton induced by an external optical pulse shows strong self-pulsing at the external-cavity round-trip time with at least ten modes excited. The numerical analysis indicates an even broader bandwidth and a transient sweep of the center frequency. It is argued that mode-locking of spatial solitons is an interesting and viable way to achieve three-dimensional, spatio-temporal self-localization and that the transients observed are preliminary indications of a transient cavity light bullet in the dynamics, though on a non negligible background.

Keywords: cavity soliton, cavity soliton laser, VCSEL, frequency-selective feedback, self-pulsing, cavity light bullet

1. INTRODUCTION

The last two years have seen rapid progress in the generation of spatially self-localized states in broad-area semiconductor lasers.[1–5] Such states represent small coherent emitters – *microlasers* – which can be controlled – i.e. switched on and off – by optical control beams.[2,6] This makes them interesting for optical information processing. These states are stabilized in the transverse plane (the one orthogonal to the cavity axis) not by boundary conditions (like mirror curvature or aperture size) but by nonlinearities, similar to a soliton. We will refer to them as *laser cavity solitons* (LCS). Indeed, they are a particular kind of *cavity solitons* (CS), bistable spatially self-localized wave packets which exist in the transverse aperture of broad-area nonlinear optical resonators (see, for example,[5,7,8]). CS and LCS have somewhat different properties from the well-known solitons in conservative systems like those of the Nonlinear Schrödinger equation (describing propagation in a Kerr medium in which the refractive index increases linearly with intensity) because of the dissipation brought about by the cavity losses (and relaxation in the medium) and the driving by external pumping (see[5,8] and Refs. therein for a review). In particular, dissipative solitons can exist and are stable in a nonlinear cavity filled with a Kerr medium in more than one space dimension,[9] in absorptive media[10] and even in defocusing media.[11]

CS in coherently driven systems[5,7] must be sustained by a beam of high temporal and spatial coherence (the so-called holding beam, HB). In contrast, *cavity soliton lasers (CSL)*, which are self-sustained, draw their energy solely from an inexpensive incoherent source, e.g. electrical pumping.[1,3] In driven systems the CS are 'slaved' because their phase, polarization and frequency is locked to that of the HB. In a CSL – as any laser – the phase is not fixed, and each LCS has the freedom to choose its own phase. Assuming that the cavity is sufficiently isotropic and broadband, the polarization and output optical frequency of each LCS is likewise undetermined. In a CSL, therefore, every single LCS within the laser aperture should have the freedom to choose its phase, frequency and polarization. This gives exciting new opportunities for fundamental studies as well as

Further author information: corresponding email: thorsten.ackemann@strath.ac.uk

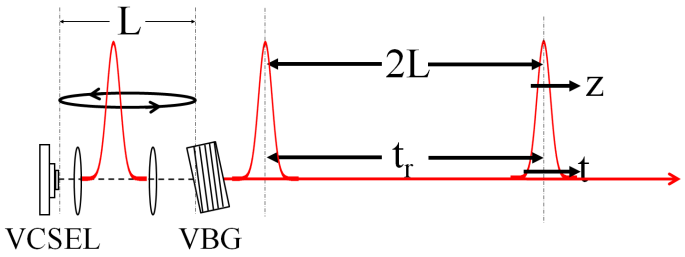

Figure 1. Scheme of a cavity soliton laser supporting cavity light bullets. Within the cavity, a pulse significantly shorter than the cavity round trip time and the cavity length is circulating. At the output coupler, it produces a train of pulses separated by the cavity round-trip time in time and by two times the cavity length in space.

for applications. For example, phase-locked multi-frequency operation would result in self-pulsing solitons which – combined with the intrinsic bistability of dissipative solitons – could be used as optically-controllable pulse trains in communication systems.

The basic idea is illustrated in Fig. 1. The scheme depicted shows a laser source with a self-imaging external cavity closed by a volume Bragg grating (VBG). In principle, the most important thing is that the cavity is long enough to allow for multi-longitudinally mode operation and is only marginally stable for Gaussian transverse modes. If a spatial (transverse) soliton operates on multiple, phase-locked cavity modes, a pulse is formed which has a duration shorter than the cavity round-trip time and is hence also spatially localized along the longitudinal (cavity) axis. This would constitute a ball or bullet of light traveling back and forth within the cavity, a *spatio-temporal or three-dimensional cavity soliton*. We will refer to it as *cavity light bullet (CLB)*. Outside the cavity, it manifests itself as a train of short pulses with the repetition frequency of the cavity round-trip time that is usual for mode-locked lasers. Indeed, the pulses in many mode-locked lasers can be understood as dissipative temporal cavity solitons, at least in many operating regimes.[8,12,13]

Light bullets or three-dimensional solitons were intensively pursued in systems without feedback, for example in,[14] but to our knowledge there is no experimental demonstration, yet. For Kerr media this is due to the fact that solitons are unstable in more than one dimension.[15] Saturation might stabilize solitons[16] but the parameter range seem to be very difficult to reach experimentally. Possible remedies are to use discrete systems,[17] approximate realizations like linear Airy-Bessel beams,[18] or cavities.[19] As we mentioned before, the dissipative dynamics of a cavity relaxes the requirements on the material to sustain CS. Indeed light bullets were found in a model for a driven cavity with a two-level nonlinearity.[19]

The first semiconductor CSL realized is built on a broad-area vertical-cavity surface-emitting laser (VCSEL) with bistability induced by frequency-selective feedback.[1,2,20–22] As such it does not have an obvious mechanism for saturable absorption to induce mode-locking. LCS or at least localized states were also demonstrated in VCSEL with saturable absorption[3,4] and indeed self-pulsing was found though not in the solitonic region.[23] Saturable absorption, however, is not the only mechanism for mode-locking. Four-wave mixing for example is known to support mode-locking in driven systems[24] and in lasers.[25] In addition, rather regular self-pulsing is known for semiconductor lasers with feedback in appropriate operating regimes.[26]

Hence, we are looking here for self-pulsing of CS in the frequency-selective feedback (FSF) scheme which has the advantage of being based on standard VCSEL structures (albeit with large diameter) and other off-the-shelf optical components without the need to grow and to align matching gain/absorber sections. We present numerical and experimental evidence in the time and spectral domain, demonstrating that a considerable number of external cavity modes are excited during a switch-on transient of a CS together with deep oscillations and self-pulsing. There is also a frequency shift of the CS during the transient. We will interpret this as the CS evolving via multi-frequency unstable states. Although the involvement of unstable separatrix states in soliton dynamics is not new, the fact that a CSL has frequency freedom means that the frequency of the separatrix and that of the final stable CS states are generally different. Hence, frequency is effectively a dynamical variable in the switching process.

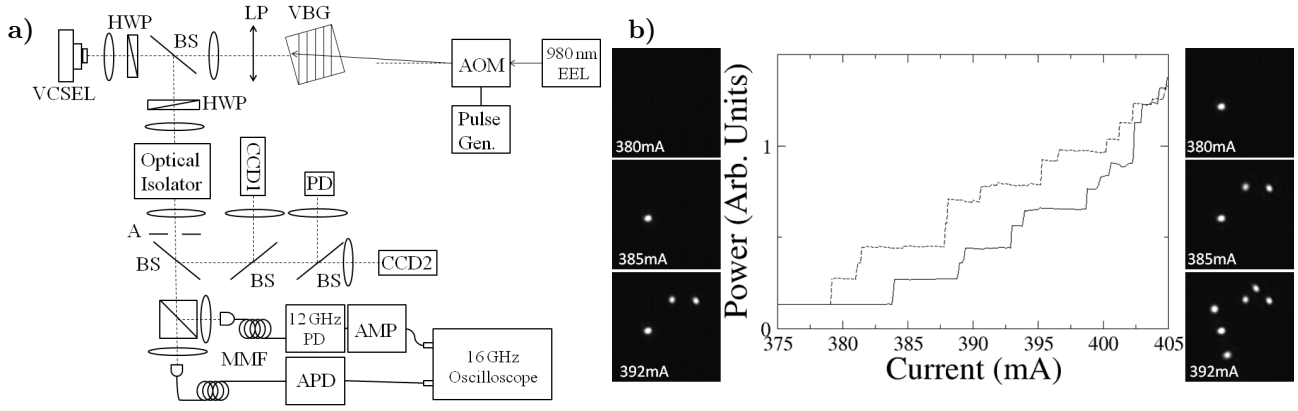

Figure 2. a) Experimental setup. VBG: Volume Bragg grating, BS: Beamsplitter, HWP: Half-wave plate, LP: Linear polarizer, M: Mirror, A: Near field aperture, MMF: Multi-mode fiber, CCD1: CCD camera in far field image plane of VCSEL, CCD2: CCD camera in near field image plane of VCSEL, PD: Photodiode, AOM: Acousto-optic modulator, APD: Avalanche photodiode, AMP: RF Amplifier. b) Typical example for the evolution of power output from the whole laser aperture with increasing (solid line) and decreasing (dashed line) current. Panels on the left (right) side correspond to near field images of the laser aperture at the inset currents for increasing (decreasing) current.

2. EXPERIMENTAL SETUP AND BASIC PHENOMENA

2.1 Experimental Setup

A schematic of the experimental setup is shown in Fig. 2a. We use a broad-area VCSEL as the nonlinear element and frequency-selective feedback to support bistability.[27] The VCSEL has a circular aperture with diameter 200 μm and a room-temperature emission wavelength of 975 nm. We heat the VCSEL to 80 °C to tune the wavelength to approach the resonance of the frequency-selective feedback, which is provided by a volume Bragg grating (VBG) with a reflectivity bandwidth of 0.2 nm and peak reflectance at 981.1 nm. The VCSEL is coupled to the VBG via a 6.25:1 magnification self-imaging cavity with an 8 mm focal length collimating lens and a 50 mm focal length lens focussing light onto the VBG. This external cavity has a longitudinal mode spacing of 950 MHz which corresponds to a round trip time of 1.05 ns which differs from the free-space round trip time due to the long intra-cavity polarizer. The self-imaging configuration maintains the high Fresnel number of the VCSEL cavity while also imposing that all waves return to their original position on the VCSEL aperture after one round trip, which is crucial to achieve spatial self-localization.

The Fresnel reflection from an uncoated glass surface is used to couple out light for detection with an out-coupling ratio of about 10% for vertically polarized light. A half-wave plate and a linear polarizer are adjusted to enforce linear polarization close to the vertical axis in order to suppress polarization instabilities[6] and optimize out-coupling. The latter is essential for time resolved measurements at high frequency due to the relatively low sensitivity of fast photodetectors and the low intrinsic power of the CS. With the intra-cavity polarizer set to transmit vertically polarized light we couple out around 15 μW of optical power per detector for a single CS.

There are two detectors for time-resolved measurements. An overview on the dynamics is obtained by an avalanche photodiode with a 3 dB cutoff frequency of 1.1 GHz and variable gain (New Focus 1647). The other is a fiber coupled photodetector with a 3 dB frequency bandwidth of 12 GHz (New Focus 1544-B) which is then amplified by a 15 dB amplifier with 15 GHz bandwidth (Picosecond pulse labs 5867). These signals are monitored on an oscilloscope with 16 GHz analogue bandwidth (LeCroy digital signal analyser) and a sampling rate of 40 Gb/s, digitally filtered at 10 GHz to reduce noise.

The detection system is isolated from the laser cavity with an optical isolator containing a Faraday rotator. An adjustable aperture is placed in a re-imaged plane of the VCSEL gain region and can be used to spatially select any area of the VCSEL, typically containing only a a single CS. The aperture size selected for single soliton measurements is typically three soliton diameters. There are charge-coupled device (CCD) cameras placed in

re-imaged near and far field planes of the VCSEL gain region and a slow photodiode for time averaged intensity measurements.

Switching the CS requires the injection of an external laser pulse. This is provided by a writing beam (WB) derived from a tunable external-grating laser diode emitting around 980 nm. The elliptically shaped laser beam is circularized by an anamorphic prism pair and passed through an acousto-optic modulator (AOM), allowing pulses to be created from a CW beam with a minimum pulse duration of 15 ns. The WB is fiber-coupled which ensures high beam quality. It is injected through the back of the VBG via steering mirrors to adjust near and far field alignment, and is demagnified. These adjustments ensure that WB at the VCSEL gain region is on axis, and its spot size matches that of a CS.

2.2 Basic Phenomena

As the current into the VCSEL is increased, there is a transition from a state of purely spontaneous emission (upper-left image of Fig. 2b) to one which has a single localized lasing spot (middle-left image of Fig. 2b). The transition is abrupt and will henceforth be referred to as an 'on-switch'. The spot has an intensity profile with circular symmetry. It is approximately Gaussian, with $1/e^2$ radius 5.3 μm. The emission from this spot is coherent, with an optical linewidth of about 6 MHz, hence it can be considered as a micro-laser. If the current is increased further we see additional spots which are very similar in size and amplitude to the original one, as illustrated in Fig. 2b. The LI-curve in Fig. 2b also shows that these structures are bistable, since for all currents between 378 mA and 403 mA there are two intensity levels. In actual fact (as Fig. 2b suggests) the system output results from the switching on and off, at different thresholds, of individually-bistable microlasers. These micro-lasers are independent from each other and each may be switched on and off without affecting the rest of the system. In other words, the system is *locally bistable, but globally multistable.*

The microlasers in the present system – as in all reported semiconductor-based realizations[2,4,7,23] – are pinned at certain locations, i.e. they can't exist at arbitrary locations within the aperture as would be expected for a perfectly homogeneous system.[5] This is believed to be due to micron-scale defects in the VCSEL structure which create preferred positions for the microlasers. For a full description of the CS in this system refer to.[6] Here, we will concentrate on the CS with the lowest threshold. Its switching threshold, switching delays and some aspects of the transient dynamics are analyzed in detail in.[28]

3. THE MODEL

To model the experimental set-up of Fig. 2, separate descriptions of the VCSEL device and the VBG are required. The temporal dynamics of semiconductor lasers with optical feedback has been modeled for some time (see for example[29]). The present experimental setup however, requires the inclusion of the transverse-space degrees of freedom, including diffraction, and also of high reflectivity of the feedback mirror. We combine all these elements in a single model that can be compared with the experimental realizations and does not restrict to purely temporal regimes and/or introduce restrictions in the magnitude of the feedback.[22]

Our model for the intra–VCSEL optical field E and carrier density N is based on that used for the study of CS in amplifiers.[7] The holding beam is, however, replaced by the external cavity field at the VCSEL output mirror, F. The complete system is described by the following system of coupled partial differential equations and mapping:[22]

$$\begin{aligned} \partial_t E &= -(1+i\theta)E + i\nabla^2 E - i\sigma(\alpha+i)(N-1)E \\ &+ \frac{2\sqrt{T_1}}{(T_1+T_2)}F \\ \partial_t N &= -\gamma\left[N - J + |E|^2(N-1) + D\nabla^2 N\right] \\ F(t) &= e^{-i\delta\tau_f}\hat{G}(t-\tau_f/2)\ \left[-r_1 F(t-\tau_f) + t_1 E(t-\tau_f)\right] \end{aligned} \tag{1}$$

where θ is the detuning of the VCSEL cavity with respect to the chosen reference frequency, σ is a coupling constant, α is the linewidth enhancement factor, T_1 and T_2 are the transmittivities of the VCSEL mirrors, and J represents the injection current, normalised to the value at transparency. Time is scaled to the VCSEL cavity

lifetime, and γ is the ratio of cavity lifetime to carrier response time in the VCSEL. The term $\nabla^2 E$ describes diffraction in the VCSEL cavity. $D\nabla^2 N$ is the carrier diffusion but it is usually considered small, and will henceforth be omitted.

The external cavity round–trip time and its detuning at the reference frequency are denoted by τ_f and δ respectively, while r_1 and t_1 are the (real) amplitude reflection and transmission coefficients of the VCSEL output mirror, (i.e. $T_1 = t_1^2 = 1 - r_1^2$). The operator $\hat{G}$ describes the frequency–selective operation of the Bragg reflector on the field envelope and is given by

$$\hat{G}(t)\ [h(t)]\ = \frac{r_g}{2\beta} \int_{t-2\beta}^{t} e^{i\Omega_g (t'-t)}\ h(t')\ dt' \tag{2}$$

in the time domain or, equivalently,

$$\hat{G}(\omega)\ [h(\omega)]\ = r_g\ e^{-i\beta(\Omega_g - \omega)}\ \mathrm{sinc}(\beta(\Omega_g - \omega)) h(\omega) \tag{3}$$

in the frequency domain. The frequency $1/\beta$ determines the bandwidth of the Bragg reflector while Ω_g is its central frequency (henceforth referred to as the Bragg frequency) relative to the reference (carrier) frequency. The parameter r_g is an overall reflection coefficient. Note that in this description we neglect the transverse wavevector dependence of the reflector response. We have also ignored transverse effects of free–space propagation (i.e. diffraction) in the external cavity, since in the corresponding experiment the VCSEL output coupler is imaged directly onto the Bragg reflector (see Fig. 2). Note that all variables and parameters in Eqs. (1) are dimensionless. We use $\Omega_g = 0$ here, i.e. the carrier frequency is chosen to be the Bragg frequency.

The model reproduces existence and stability of LCS in qualitative agreement with experiment.[22] Switching thresholds vs. pulse duration and switching delays were analyzed in[28] and also found to be in good qualitative agreement with experiment.

4. CAVITY SOLITON DYNAMICS

4.1 Experimental results

In the section, we are analyzing the self-pulsing after a switch-on of a CS by the WB. The wavelength of the WB is about 0.1 nm blue detuned to the wavelength of the emerging CS which was found to minimize switching powers.

Fig. 3a shows the response of the system to a 50 ns pulse with threshold peak power. There is a delay of 5-10 ns after the end of the pulse until the CS switches on. Then there is strong, fairly regular pulsing with a repetition frequency of 950 MHz, which is the cavity-round-trip frequency. In between, especially in the interval between 75 and 80 ns, there is fast pulsing in between the main pulses. Then, starting at about 85 ns, the envelope of the pulsing becomes smaller whereas the frequency seems to increase. Furthermore, there is a transition from an asymmetric pulsing state to a more symmetric one. This tendency continues until at long times there seems to be a noisy oscillation around a mean value, the DC values of the switched-on CS (about 30 mV, Fig. 3b).

The noise present within the large bandwidth of the detection limits the signal to noise ratio, making direct time trace analysis sometimes, e.g. in Fig. 3b, difficult. For a clearer analysis, a time-frequency spectrogram is used (Fig. 3c). This is simply a time evolving Fourier transform of the time series with overlapping time windows. Low frequencies are not shown since at switch-on the DC contribution dominates and would swamp the oscillation peaks. The spectrogram shows clearly that the dynamics are dominated by the external cavity round trip frequency (950 MHz) and its harmonics spanning over the whole detection bandwidth. The strongest frequencies are the second and third harmonic at 1.9 GHz and 2.85 GHz but all harmonics up to 10 GHz are excited. Apparently all or significant parts of these oscillations are in phase, leading to the pronounced self-pulsing in the time domain, i.e. mode-locking. After about 50 ns, the spectrogram starts to simplify, the low and high harmonics die out whereas the ones around 3-6 GHz persist to about 250 ns. This state corresponds to the weakly modulated oscillatory state in Fig. 3b. The first reason that the pulsing disappeared is that there

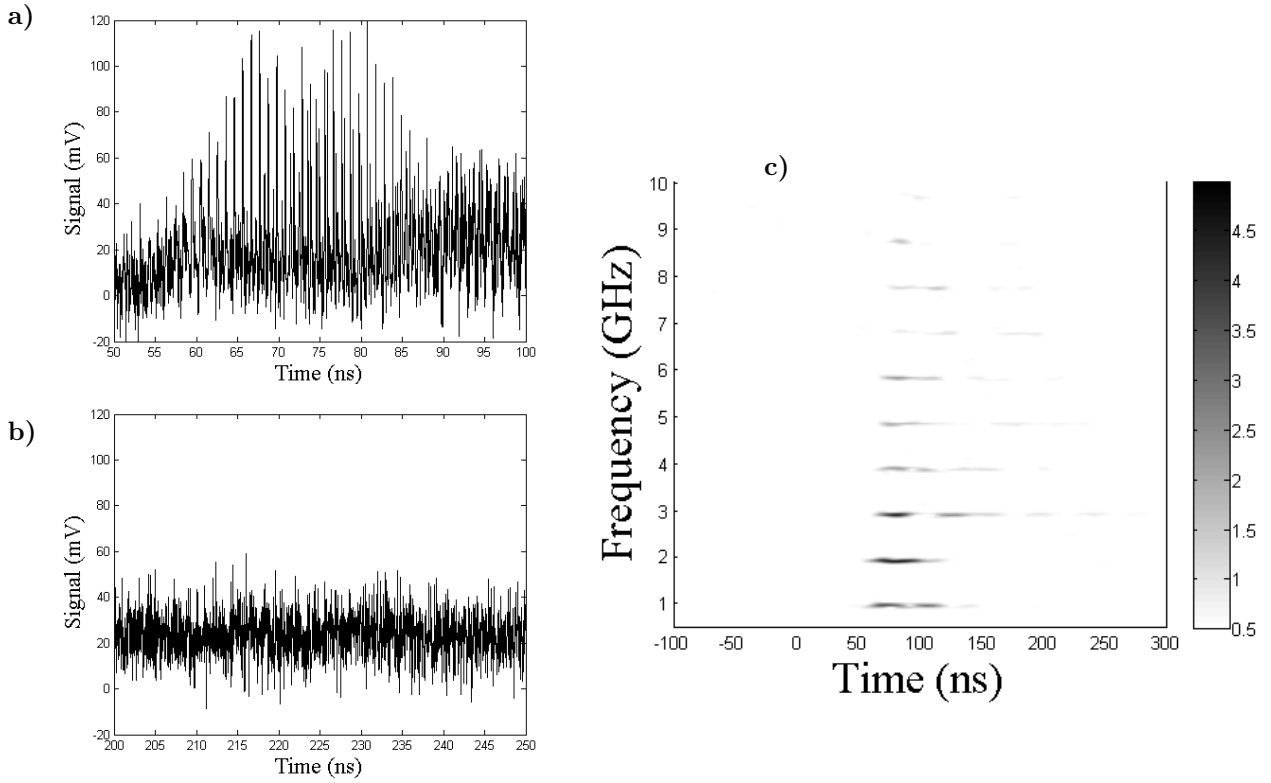

Figure 3. Switch-on transient of a CS initiated by a 50 ns pulse of minimum threshold power. a) Transient regime with strong pulsing. b) Quasi-cw state at later times. c) Time-frequency spectrogram of intensity time series (Fourier window of 25.6 ns). Negative times correspond to the off state, before the pulse is applied.

are less harmonics, probably the second that the phase-locking is lost. Finally, for these parameters, the system relaxes to a non-oscillatory steady on-state.

It is interesting to note that also the envelope of each harmonic is modulated and that there is some tendency that the modulation is in anti-phase between different component (e.g. around 100 ns the 3 GHz component has a minimum whereas the 1 GHz one a maximum; the 4 and 6 GHz components have a maximum around 150 ns whereas the 7 and 8 GHz are minimal). This can be interpreted as a change in excitation between different external cavity modes leading to the dominance of particular beat notes/harmonics.

If the pulse power is increased, the switch-on delay becomes smaller and pulsations start already during the WB pulse.[28] Fig. 4a shows the situation for a pulse with 4.8 times threshold power. At that amplitude, there is no discernible switch-on delay and pulsing begins at the start of the pulse. When the pulse ends, the dominant harmonic shifts, and the intensities of the peaks reduce (Fig. 4c). The evolution again shows the reduction of oscillating harmonics until the system simplifies into one or two frequencies. The system does not relax to a non-oscillating state in this case, however, as the component at 3.8 GHz remains. These states may show long-term stable oscillations, whose properties are currently under further investigation. It should be noticed that the long-term behavior of the system is not only determined by initial conditions but also by noise. A fluctuation can cause the oscillating state to decay to a non-oscillatory CS state and, vice versa, a steady state can 'spontaneously' convert to an oscillating state on long time scales (ms to minutes or hours).

4.2 Numerical Simulations

We have investigated in detail the soliton writing process in the model (1), mimicking the experimental procedure described in Section 4.1. We initiate a CS through the application of a spatially–localized rectangular WB pulse

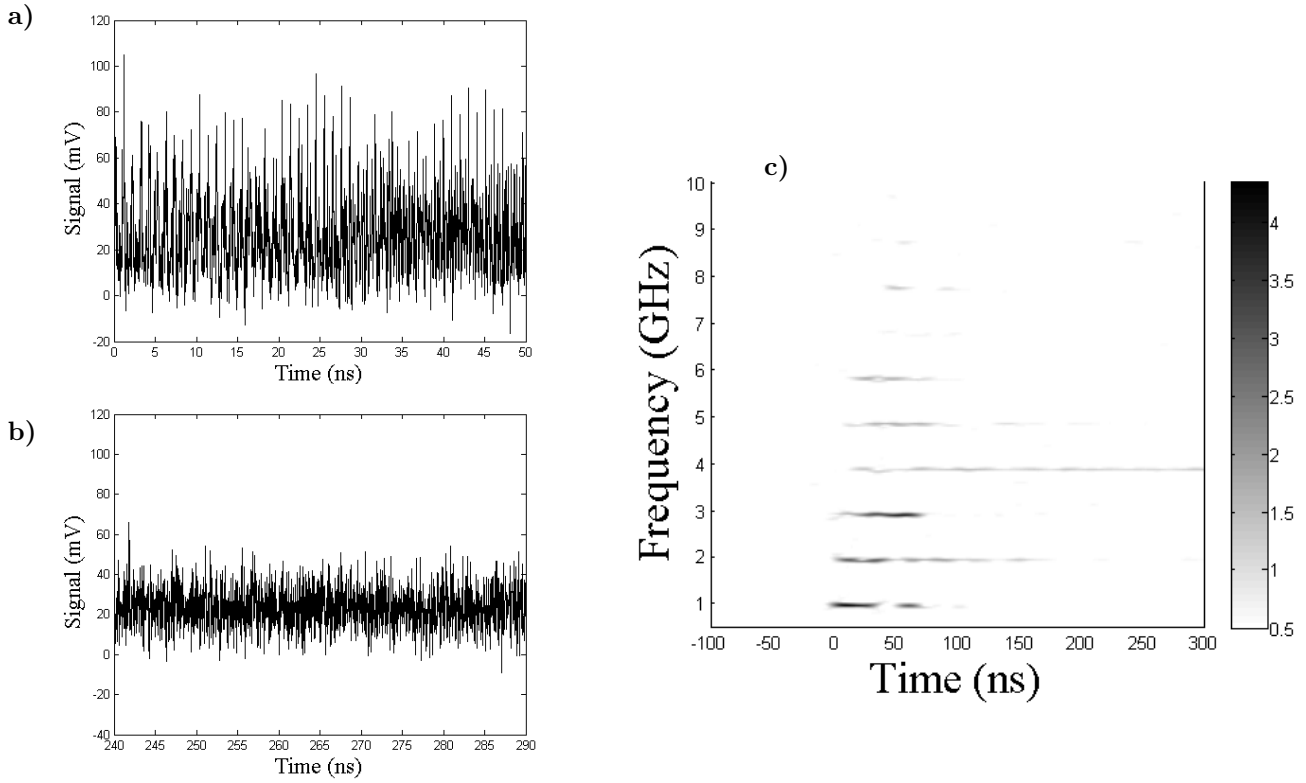

Figure 4. Switch-on transient of a CS initiated by a 50 ns pulse of 11.8 times minimum threshold power. a) Transient regime with strong pulsing. b) Quasi-cw state at later times. c) Time-frequency spectrogram of intensity time series.

$A(x,t)$ of the form

$$A(x,t) = A_0 \exp\left(-\frac{x^2}{\eta^2} - i\omega_p t\right) \mathrm{rect}\left(\frac{t}{\tau_p}\right). \tag{4}$$

Computationally, the WB is added to the first of Eqs. (1) while the amplitude A_0, width η, duration τ_p and frequency ω_p of the address pulse can all be varied. The parameters are: $\alpha = 9$, $\theta = -1$, $\sigma = 0.9$, $\gamma = 0.01$, $T_1 = 0.008$, $T_2 = 0.0002$, $\beta = 0.6$, $r_g = 0.8$, $\delta = 0$, $\tau_f = 41$, $\eta = 5$, and $\tau_p = 2000$. Assuming a typical cavity decay time of $1/\kappa = 10$ ps, the cavity round-trip time is 0.41 ns, the repetition rate 2.4 GHz, about two times the value used in the experiment. We fix the value of the address pulse duration at around 50 round trips of the external cavity (i.e. around 20 ns). The optimal frequency shift for which the lowest-amplitude address pulses can generate a CS is found to be around $\omega_p = 3.5$ corresponding to around 55 GHz or 0.18 nm in experimental values, in qualitative agreement with the experimental finding.

The numerical integration of the model (1) provides temporal data on the *field* dynamics of the CS switching. As in the experiment, we display first the intensity time series directly and evaluate time-frequency spectrograms. Fig. 5a shows strong self-pulsing at the switch-on which starts during but towards the end of the WB pulse. It is dominated by the round-trip frequency (being about two times faster than in the experiment due to the choice of parameters). In addition, there is a low-frequency envelope. Sometimes we observe experimentally transient (as well as persistent) modulations on the 100 to 20 MHz scale in the total intensity too. These are possibly related to a Q-switching instability typical for class-B lasers and noted – at least for the transient – also for CSL with saturable absorbers.[4,30] The appearance of low-frequency fluctuations is also typical for semiconductor lasers with feedback in general (see for example[26,29]).

The spectrogram in Fig. 5c shows strong excitation of the fundamental round-trip frequency and harmonics (we choose to cut it at 20 GHz to mimic the experimental cut-off at about 10 harmonics). The dynamics then simplifies with the components around 5 GHz becoming dominant. This corresponds to a small-amplitude

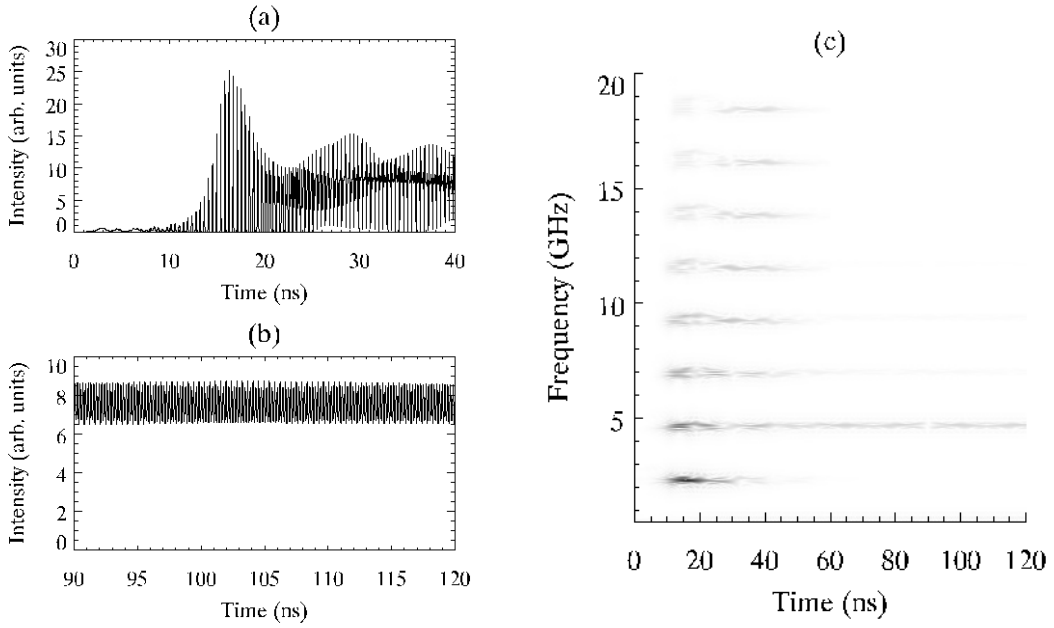

Figure 5. Numerical simulation of a switch-on transient of a CS initiated by a 20 ns pulse of 2.3 times minimum threshold power. a) Initial transient regime with strong pulsing. b) Weakly oscillating state at later times. c) Time-frequency spectrogram of intensity time series (Fourier window of 8 ns; each time window is normalized separately for contrast enhancement).

oscillation around the DC value of the CS (Fig. 5b). These findings are in very good qualitative agreement with experiment.

In the simulations, it is also rather straightforward to compute a time-resolved optical spectrum, i.e. the Fourier transform of the field $E(x = 0, t)$, which is difficult in the experiment. Fig. 6a shows the spectrogram with a time window of one round-trip for the individual Fourier transforms. The WB pulse is apparent in the first 20 ns around 55 GHz. Already before the end of the address pulse, multi-mode operation sets in. At 10 ns from the beginning of the simulation, around 30 external cavity modes are present. This regime of frequency spreading is followed by a fast (around 5 ns) sweeping of the frequency spectrum towards the Bragg frequency at zero, accompanied by a narrowing to only about 15 modes. Then slower spectral evolution leads to a further narrowing of the spectrum and to the final state of the CS, which has one strong external-cavity mode slightly red detuned to the Bragg frequency with two side modes at ± 5 GHz (plus some even weaker side modes). This is in accordance with the dynamics of the intensity spectra, of course. It should be noted that the survival of a single line in the field spectrum denotes cw emission whereas the presence of a single line in the intensity (RF) spectrum denotes an oscillation.

Surprisingly, very similar spectral dynamics take place when the WB frequency is close to that of the final CS (Fig. 6b). In this case, the writing beam corresponds to $\omega_p = 0$ and yet one still observes the same three distinct dynamical regimes: creation of a band of modes close to 55 GHz, followed by a fast spectral broadening and frequency sweep, and finally a slower spectral narrowing to a quasi-single-mode CS emission state. Apart from a longer duration of the first phase, this spectral evolution is remarkably similar to that observed in Fig. 6a. This suggests the existence of a globally attractive, yet unstable, oscillatory state that is initially approached, independently of the frequency of the WB. This state still corresponds to spatial localization, since the CS is well defined during the entire duration of the transient. Another interesting feature of Fig. 6 is that the first frequency response of the system takes place around the blue-detuned frequency of the minimum threshold determined before, again independently of the frequency shift ω_p of the addressing beam. This seems to correspond to the unstable low-amplitude CS state typically found in CSL models,[20–22] which is likely to behave like a separatrix in CS switch-on.

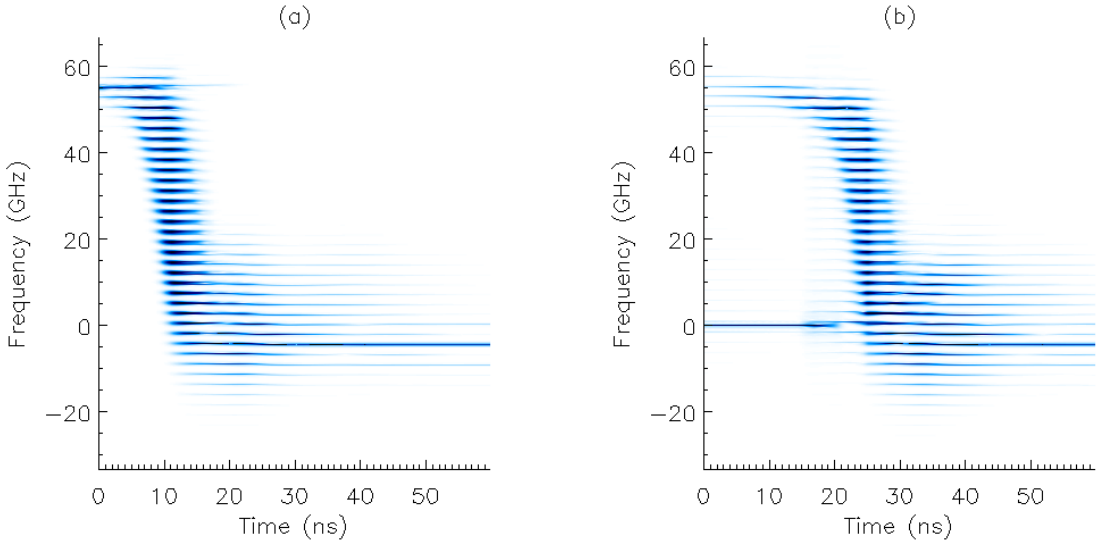

Figure 6. (Color online) Time evolution of the field frequency spectrum evaluated every round trip. a) $\omega_p = 3.5 \equiv 55$ GHz, b) $\omega_p = 0$. Each frequency spectrum is normalized such that the highest intensity corresponds to dark blue (black), to avoid the dominance of the final peak.

5. CONCLUSION

The transient of a switch-on of a CS in a CSL based on FSF is accompanied by pronounced self-pulsing at the cavity round-trip time and the excitation of a large number of external cavity modes. In addition, there is a shift of the carrier frequency highlighting the importance of unstable, multi-frequency soliton states to organize the transient dynamics. This frequency sweeping has no counterpart in VCSELs with optical injection such as, for example, that of.[7,31] More generally, a CSL without holding beam has the freedom to change frequency. Similar phenomena might exist in the schemes relying on saturable absorption[3,23] due to phase-amplitude coupling.

The occurrence of pronounced, fairly regular pulsing indicates that these modes are at least partially phase-locked, i.e. there is transient mode-locking of spatial LCS. In the present stage we cannot give quantitative information on the modulation depth but the very existence of pulses indicates the existence of structures significantly shorter than the cavity round-trip time. Hence, we conclude that the initial phase of switch-on is characterized by (transient) cavity light bullets, probably on an irregular non-zero background.

In some realizations, a transition to an asymptotically stable oscillating or pulsing state is observed. This is a very exciting observation because it indicates the possibility of achieving simultaneous spatial and temporal self-localization via mode-locking of spatial solitons at different external cavity modes. Such features of CS in VCSELs with FSF are under current investigation.

Acknowledgements

This work was partially supported by EU FP7 ICT FET Open HIDEAS and in the initial phases by the EU FP6 STREP FunFACS. NR and CM are supported by an EPSRC doctoral training account. We are grateful to A. J. Scroggie for his contributions to the modeling and to R. Jäger from Ulm Photonics for supplying the devices.

REFERENCES

1. Y. Tanguy, T. Ackemann, W. J. Firth, and R. Jäger, "Realization of a semiconductor-based cavity soliton laser," *Phys. Rev. Lett.* **100**, p. 013907, 2008.

2. Y. Tanguy, N. Radwell, T. Ackemann, and R. Jäger, "Characteristics of cavity solitons and drifting excitations in broad-area vertical-cavity surface-emitting lasers with frequency-selective feedback," *Phys. Rev. A* **78**, p. 023810, 2008.
3. P. Genevet, S. Barland, M. Giudici, and J. R. Tredicce, "Cavity soliton laser based on mutually coupled semiconductor microresonators," *Phys. Rev. Lett.* **101**, p. 123905, 2008.
4. T. Elsass, K. Gauthron, G. Beaudoin, I. Sagnes, R. Kuszelewicz, and S. Barbay, "Fast manipulation of laser localized structures in a monolithic vertical cavity with saturable absorber," *Appl. Phys. B* **98**, pp. 327–331, 2010.
5. T. Ackemann, G.-L. Oppo, and W. J. Firth, "Fundamentals and applications of spatial dissipative solitons in photonic devices," *Adv. Atom. Mol. Opt. Phys.* **57**, pp. 323–421, 2009.
6. N. Radwell and T. Ackemann, "Characteristics of laser cavity solitons in a vertical-cavity surface-emitting laser with feedback from a volume Bragg grating," *IEEE J. Quantum Electron.* **45**, pp. 1388–1395, 2009.
7. S. Barland, J. R. Tredicce, M. Brambilla, L. A. Lugiato, S. Balle, M. Giudici, T. Maggipinto, L. Spinelli, G. Tissoni, T. Knödel, M. Miller, and R. Jäger, "Cavity solitons as pixels in semiconductors," *Nature* **419**, pp. 699–702, 2002.
8. N. Akhmediev and A. Ankiewicz, *Dissipative solitons*, vol. 661 of *Lecture Notes in Physics*, Springer, Berlin, 2005.
9. W. J. Firth and A. Lord, "Two-dimensional solitons in a Kerr cavity," *J. Mod. Opt.* **43**, pp. 1071–1077, 1996.
10. W. J. Firth and A. J. Scroggie, "Optical bullet holes: robust controllable localized states of a nonlinear cavity," *Phys. Rev. Lett.* **76**, pp. 1623–1626, 1996.
11. D. Michaelis, U. Peschel, and F. Lederer, "Multistable localized structures and superlattices in semiconductor optical resonators," *Phys. Rev. A* **56**, pp. R3366–R3369, 1997.
12. K. Tamura, L. E. Nelson, H. A. Haus, and E. P. lppen, "Soliton versus nonsoliton operation of fiber ring lasers," *Appl. Phys. Lett.* **64**, pp. 149–151, 1994.
13. R. Paschotta, R. Häring, A. Garnache, S. Hoogland, A. C. Tropper, and U. Keller, "Soliton-like pulse-shaping mechanism in passively mode-locked surface-emitting semiconductor lasers," *Appl. Phys. B* **75**, pp. 445–451, 2002.
14. F. W. Wise and P. Di Trapani, "The hunt for light bullets – spatiotemporal solitons," *Opt. Photon. News* **13**(2), pp. 28–32, 2002.
15. Y. Silberberg, "Collapse of optical pulses," *Opt. Lett.* **15**, pp. 1282–1284, 1990.
16. J. M. Soto-Crespo, P. Grelu, and N. Akhmediev, "Optical bullets and "rockets" in nonlinear dissipative systems and their transformations and interactions," *Opt. Exp.* **14**, pp. 4013–4025, 2006.
17. D. Mihalache, D. Mazilu, F. Lederer, and Y. S. Kivshar, "Spatiotemporal dissipative solitons in two-dimensional photonic lattices," *Phys. Rev. E* **78**, p. 056602, 2008.
18. A. Chong, W. H. Renninger, D. N. Christodoulides, and F. W. Wise, "AiryBessel wave packets as versatile linear light bullets," *Nature Phot.* **4**, pp. 103–106, 2010.
19. M. Brambilla, T. Maggipinto, G. Patera, and L. Columbo, "Cavity light bullets: Three-dimensional localized structures in a nonlinear optical resonator," *Phys. Rev. Lett.* **93**, p. 203901, 2004.
20. P. V. Paulau, A. J. Scroggie, A. Naumenko, T. Ackemann, N. A. Loiko, and W. J. Firth, "Localized traveling waves in vertical-cavity surface-emitting lasers with frequency-selective optical feedback," *Phys. Rev. E* **75**, p. 056208, 2007.
21. P. V. Paulau, D. Gomila, T. Ackemann, N. A. Loiko, and W. J. Firth, "Self-localized structures in vertical-cavity surface-emitting lasers with external feedback," *Phys. Rev. E* **78**, p. 016212, 2008.
22. A. J. Scroggie, W. J. Firth, and G.-L. Oppo, "Cavity soliton laser with frequency selective feedback," *Phys. Rev. A* **80**, p. 013829, 2009.
23. P. Genevet, B. Barland, M. Giudici, and J. R. Tredicce, "Stationary localized structures and pulsing structures in a cavity soliton laser," *Phys. Rev. A* **79**, p. 033819, 2009.
24. P. DelHaye, A. Schliesser, O. Arcizet, T. Wilken, R. Holzwarth, and T. J. Kippenberg, "Optical frequency comb generation from a monolithic microresonator," *Nature* **450**, pp. 1214–1217, 2007.

25. J. Renaudier, R. Brenot, B. Dagens, F. Lelarge, B. Rousseau, F. Poingt, O. Legouezigou, F. Pommereau, A. Accard, P. Gallion, and G.-H. Duan, "45 GHz self-pulsation with narrow linewidth in quantum dot Fabry-Perot semiconductor lasers at 1.5 μm," *Electron. Lett.* **41**, pp. 1007–1008, 2005.
26. T. Heil, I. Fischer, W. Elsäßer, B. Krauskopf, K. Green, and A. Gavrielides, "Delay dynamics of semiconductor lasers with short external cavities: Bifurcation scenarios and mechanisms," *Phys. Rev. E* **67**, p. 066214, 2003.
27. A. Naumenko, N. A. Loiko, M. Sondermann, K. F. Jentsch, and T. Ackemann, "Abrupt turn-on and hysteresis in a VCSEL with frequency-selective optical feedback," *Opt. Commun.* **259**, pp. 823–833, 2006.
28. N. Radwell, C. McIntyre, A. J. Scroggie, G.-L. Oppo, W. J. Firth, and T. Ackemann, "Switching spatial dissipative solitons in a VCSEL with frequency-selective feedback," *Eur. Phys. J. D* **59**, pp. 121–131, 2010.
29. B. Krauskopf and D. Lenstra, *Fundamental issues of nonlinear laser dynamics*, vol. 548 of *AIP Conference Proceedings*, American Institute of Physics, Melville, 2000.
30. K. Mahmoud Aghdami, F. Prati, P. Caccia, G. Tissoni, L. A. Lugiato, R. Kheradmand, and H. Tajalli, "Comparison of different switching techniques in a cavity soliton laser," *Eur. Phys. J. D* **47**, p. 447455, 2008.
31. X. Hachair, F. Pedaci, E. Caboche, S. Barland, M. Giudici, J. R. Tredicce, F. Prati, G. Tissoni, R. Kheradmand, L. A. Lugiato, I. Protsenko, and M. Brambilla, "Cavity solitons in a driven VCSEL above threshold," *IEEE J. Sel. Top. Quantum Electron.* **12**, pp. 339–351, 2006.